Advanced Lab Course
University of Göttingen

FM.ULP

Spatial and Temporal Distortions of Ultrashort Light Pulses

Zeitliche und räumliche Verzerrung von ultrakurzen Lichtpulsen

---

Name:	Torben Purz
E-Mail:	torben.purz@stud.uni-goettingen.de
Conducted On:	08.11.2017
Conducted with:	Hannes Paul Hoeppe Johannes Otto
Assistant:	Dr. Sabine Steil

Submission

Date: 29.11.2017 Signature of assistant:

Review

Date:	Name of Examiner:
Points:	Signature
Mark:	

Contents

1. Introduction

The upcoming of femtosecond science coincides with the ability to build lasers emitting pulses in this specific time regime. It gave rise to many scientific applications from femtochemistry, being awarded the nobel prize in 1999 [1], to the generation of even shorter pulses such that time-resolved experiments with a temporal resolution in the attosecond regime can be performed [2]. Many processes we would rather describe as instantaneous happen on this short time scale and are now available via pump-probe experiments.

Moreover, the high intensities available with ultrashort pulses gave birth to a whole new field of nonlinear optics, containing schemes like high-harmonic generation [3], which provide a competitive table-top-source to Synchrotons in the soft x-ray regime. Besides the mere scientific application, industrial application, e.g., for micro-machining [4], makes ultrashort pulses more than ever relevant for our current society.

Undoubtful, the handling of ultrashort laser pulses comes with several issues which have to be controlled, most importantly temporal and spatial pulse distortions. This distortions are only relevant for ultrashort pulses as they are especially sensitive towards these effects either by their short duration or their large spectral bandwidth [5].

In this experiment, several causes of distortion, by further examining the effects of different mirror types, transmissive glasses (tilted and untilted) as well as lenses and prisms, should be examined. The resulting pulses are measured with the GRENOUILLE technique, introduced by Trebino *et al.* in 2001 [6], extracting the full electric field in the temporal and frequency domain, as well as pulse-front tilt and spatial chirp of the pulses. The reasons for the occuring distortions will be discussed theoretically and the experimental data will be compared to simulated data using the different software and an own algorithm.

The experiment thus instructs in several crucial techniques for optical laboratory work, which is a generally interdisciplinary field ranging from biology and chemistry to physics. Especially knowledge about the effects of optical elements along the beampath on the ultrashort pulses is inevitable knowledge for every scientist studying ultrafast phenomena.

2. Theory

In general, light and its propagation through a medium or vacuum can be described by the three dimensional wave-equation

$$\left({v_{ph}}^2 \nabla^2 - \frac{\partial^2}{\partial t^2} \right) \mathbf{E} = 0, \tag{1}$$

where v_{ph} denotes the phase velocity of the wave, t the time and $\mathbf{E}$ the electric field. Using the linearity of Maxwell's equations from which equation (1) can be derived, the solutions of the wave equation can be decomposed spectrally. In optics, often instead of using sine or cosine, a complex exponential function in the form

$$\mathbf{E}(\mathbf{r}, t) = \mathbf{E_0} e^{i(\omega t - \mathbf{k}\cdot\mathbf{r} + \phi_0)}, \tag{2}$$

is favored. Here, $\mathbf{E_0}$ denotes the amplitude of the electric field, ω the frequency, $\mathbf{k}$ the wavevector, $\mathbf{r}$ the spatial position and φ_0 an initial phase. However, only the real part of equation (2) is a physical solution and the complex form is used simply for convenience.[7]

So far, only monochromatic waves have been regarded, and the amplitude is time-independent which led to the term *continous wave* (cw) mode.

By superimposing solutions for different frequencies, one can obtain so-called wave packages being localized in the temporal domain, with the gaussian wave packet being undoubtfully the most famous representative and the temporal envelope of the electric field becomes time dependent. In the following we apply the scalar approximation [8], in which only one spatial dimension, chosen to be x, is of interest and reduces the vectorial field $\mathbf{E}$ to a scalar one. Even further, the spatial dependence of the wave is of secondary interest and thus dropped for reasons of convenience.

2.1. Mathematical description of ultrashort laser pulses

Ultrashort pulses are often described by neglecting the oscillatory part and regarding the temporal envelope. They can generally be represented in the temporal domain by its pulse envelope and its temporal phase or in frequency domain by the spectral amplitude and the spectral phase. Hence, the pulses can be generally be described by

$$E(t) = A(t) \cdot e^{i\phi(t)} \qquad \tilde{E}(\omega) = \tilde{A}(\omega) \cdot e^{i\varphi(\omega)}, \tag{3}$$

equivalentily [9].

The most important aspect is that both amplitude and phase are crucial for a full retrieval of the pulses properties. The respective representations in the temporal and frequency domain can be converted, as seen in [9, p.13], by a simple Fourier transform

$$\tilde{E}(\omega) = \mathcal{FT}(E(t))(\omega) = \frac{1}{\sqrt{2}} \int_{-\infty}^{\infty} E(t) e^{-i\omega t}.$$

The most common pulse shapes in the temporal domain are the gaussian pulse ($E(t) \propto \exp[-2\ln(2)t^2/\tau^2]$) and the sech^2 pulse ($E(t) =\propto 1/\cosh^2(t/\tau)$), where τ denotes the pulse duration. The usual convention is the Full width at half maximum (FWHM). Another typical quantity for a simplified description of pulses is the bandwidth in the frequency domain which refers to the FWHM of the Spectrum which is given by the intensity envelope of the pulses spectral representation.

An important aspect connected to the relation of time and frequency domain is the so-called Fourier limit, denoting the minimum pulse duration achievable for a given spectrum. It can only be retrieved in the case of a flat spectral phase, as elucidated below. In this case, for different pulse shapes, the Fourier limited pulse duration can be calculated from the time-bandwidth product

$$\Delta\nu\Delta t \geq K\,, \tag{4}$$

where K is a number only depending on the shape of the pulse, $\Delta\nu$ the bandwidth of the pulse ($\omega = 2\pi\nu$) and Δt the temporal bandwidth or pulse duration. For a Gaussian pulse shape, K can be determined to be 0.441 according to [10].

As mentioned previously, the pulse can be described by its spectrum, its spectral phase and is minimal for a frequency independent spectral phase. When propagating through air, the refractive index is assumed to be constant and equal to one yielding a frequency independent phase change, however, when propagating through a medium like glass, the phase

$$\varphi(\omega) = k(\omega)\cdot d = k_0 \cdot d \cdot n(\omega),$$

is added in the frequency domain, with k_0 being the initial wavevector for the central wavelength. It is wavelength dependent due to the wavelength dependence of the refractive index, given by the Sellmeier equation [11]

$$n^2(\lambda) = 1 + \frac{B_1\lambda^2}{\lambda^2 - C_1} + \frac{B_2\lambda^2}{\lambda^2 - C_2} + \frac{B_3\lambda^2}{\lambda^2 - C_3},$$

where B_i and C_i are material specific constants. Thus, the wavelength λ and accordingly the wavenumber $k = 2\pi/\lambda$ are also wavelength dependent. This is often a limiting factor or at least a factor to be considered in ultrafast experiments.

The spectral phase is commonly seperated into different contributions by using a taylor expansion [12]

$$\varphi(\omega) = \varphi_0 + \varphi_1(\omega - \omega_0) + \frac{\varphi_2}{2}(\omega - \omega_0)^2 + \frac{\varphi_3}{6}(\omega - \omega_0)^3 + \mathcal{O}((\omega - \omega_0)^4). \tag{5}$$

The constant phase has no effect on the time domain representation of the pulses envelope, wherefore it is not of interest here. For pulses which have durations close to one optical cycle however, this is of interest as it describes a phase shift between oscillation and envelope which becomes notable in the case of few oscillations per envelope.

Mathematically speaking, a linear phase in the frequency domain leads to a displacement in the time domain, using the Fourier displacement theorem. Therefore, also the linear phase term is not affecting the pulse shape in time domain. Physically speaking, as the group velocity is defined as [13]

$$v_g = \frac{1}{\frac{\partial k}{\partial \omega}}, \tag{6}$$

and as $\phi \propto k$ a linear phase leads to a non-vanishing, but constant group velocity. As one compares the propagated pulse with the initial pulse, the propagated pulse arrives later due to the different group velocity. This can be observed as a shift in time, connecting the physical conception to the mathematical theorem.

The quadratic term in equation (5), commonly known as Group delay dispersion (GDD), and with several proportionality factors often refered to as *chirp*, is relevant for pulse compression. Looking back to equation (6), one can easily observe, that a quadratic phase leads to a linear behaviour in the derivative of k and therefore to $v_g \propto 1/(\omega - \omega_0)$. As the group velocity is frequency dependent, the different spectral parts of the pulse travel with a different group velocity and the pulse will disperse, leading to temporal stretching. While the GDD characterizes the pulse, materials are often classified by their Group velocity dispersion (GVD), which is given by the GDD added to the spectral phase per mm of traversed material. It can also be expressed as

$$\mathrm{GVD} = \left(\frac{\mathrm{d}^2 k(\omega)}{\mathrm{d}\omega^2} \right) \Bigg|_{\omega_0}.$$

The third term in equation (5), φ_3, denotes the third-order dispersion (TOD).

In most cases, where the compression is limited by second order contributions, the achievable pulse duration is given by [5]

$$\Delta t_{out} = \frac{\sqrt{\Delta t^4 + 16(\log 2)^2 {\varphi_2}^2}}{\Delta t}. \tag{7}$$

This directly underscores, that the shorter the pulse, the more sensitive it is to distortion of its spectral phase.

2.2. Spatial distortions of ultrashort laser pulses

Besides temporal distortions, often noted as effects on the spectral phase as described above, also spatial distortions notably influence ultrashort laser pulses. The two most common spatial distortions are pulse-front tilt and spatial chirp.

2.2.1. Spatial chirp

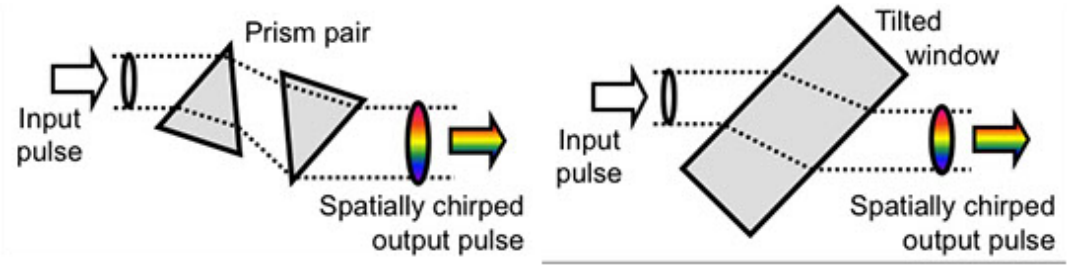

Figure 1: Causes for spatial chirp [14]

Spatial chirp, very similar to temporal chirp, which means that different wavelengths can be found at different times, denotes the effect that the wavelength distribution varies spatially across the beam. Generally, spatial chirp arises from angular dispersion for non-perpendicular incidence [8], as dictated by Snell's Law. It thus can occur in a pair of prism. Moreover, it can also occur if a tilted window is traversed by the optical pulse, again following from Snell's law where shorter wavelengths tend to refract closer to the surface normal. It is hence expected that the sign of the spatial chirp changes if the plate is tilted in a different direction.

2.2.2. Pulse-front tilt

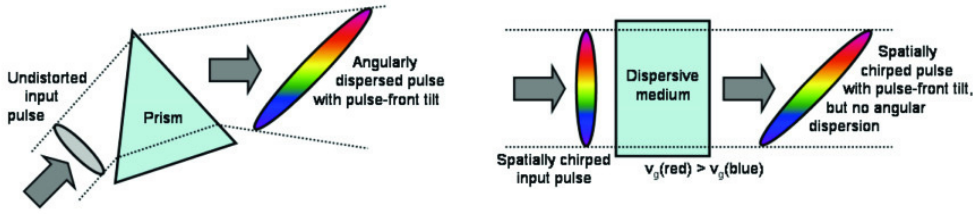

Figure 2: Causes for pulse-front tilt when using ultrashort laser pulses [15].

Pulse-front tilt, having a very figurative name, describes the phenomena that the pulse-front is tilted with respect to the propagation direction, thus the arrival time of the pulse varies along the beam-profile. It can either be caused by a prism or grating[1], or as shown by Trebino *et. al* in 2004 [15], by a spatially chirped pulse entering a material. As different wavelengths have a different velocity while propagating through the material, the pulsefront will eventually tilt.

[1] As this is not of interest in this work because no grating has been used, the author decided to drop the detailed graphical elucidation.

Both effects are especially important for ultrashort laser pulses, as a short pulse corresponds to a broad spectrum. If perfectly aligned, spatial chirp should not occur in a prism compressor, however it is very likely that at least a small amount occurs due to subtle suboptimalities in the alignment. [16]

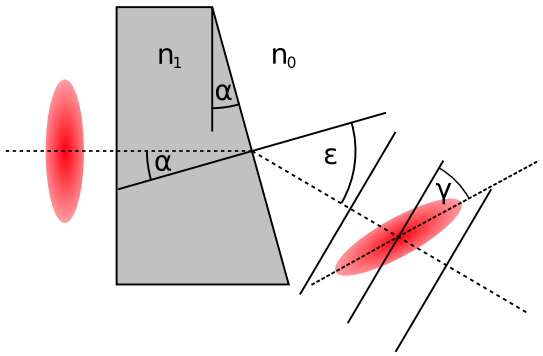

Figure 3: Geometric construction for the derivation of the pulse-front tilt caused by a wedge in the beam path.

As shown in [17], the pulse-front tilt can be given in the form of the angle between pulse-front and phase-front

$$\tan(\gamma) = \lambda_0 \left.\frac{\mathrm{d}\epsilon}{\mathrm{d}\lambda}\right|_{\lambda_0} . \tag{8}$$

In the case of incidence perpendicular to the surface, the angular dispersion can easily be derived from Snellius law

$$\epsilon = \arcsin\left(\sin(\alpha) \cdot n_1(\lambda)\right), \tag{9}$$

with α being the incidence angle inside the prism as shown in Fig. 3. Combining the two equations, the resulting expression reads

$$\tan(\gamma) = \frac{\lambda_0 \sin(\alpha) \left.\frac{\mathrm{d}\epsilon}{\mathrm{d}\lambda}\right|_{\lambda_0}}{\sqrt{1 - \sin^2(\alpha) {n_1}^2(\lambda_0)}}. \tag{10}$$

Although this still leaves us with a calculable result, we want to transform it into the units fs/mm, where the femtoseconds characterize an optical path difference along the propagation distance given by a temporal delay and the mm correspond to a lateral distance x. From this, we can easily derive the pulse-front tilt given in fs/mm to be

$$\mathrm{PFT}[\mathrm{fs/mm}] = \frac{\Delta t}{x} = \tan(\gamma)/c. \tag{11}$$

2.3. Lenses and mirrors

When employing lens telescopes in a setup using ultrashort pulses, several flaws have to be considered. For large beams, the effective thickness of the lens a part of the beam is affected by might vary, depending on the distance of the optical axis. This subsequently leads to a different GDD added to different parts of the beam, yielding a non-homogenous pulse duration distribution along the beam profile. More importantly, the linear part of the phase might also differ which leads to a temporal delay between different parts of the pulses which reduces the intensity at hand and could elicit problems in time-resolved experiments.

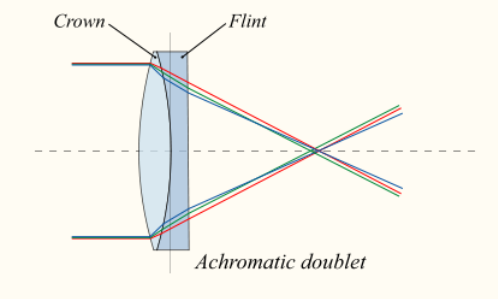

Figure 4: Setup and principle of an achromat or achromatic lens [18].

Furthermore, this will be the most notable effect, lenses contain an inherent achromatism. The refractive index differs for different wavelengths and thus the focal length does. Eventually, this could yield a telescope setup only for certain wavelengths, as other wavelengths might due to this difference of the focii diverge after traversing the two lenses.

While normales lenses, focus different wavelenghts to different focal points, an achromat eliminates this issue by combining a convex and a biconcave lens such that all wavelengths are focussed to the same point, as seen in Fig. 4. As a positive and a negative lens are used as well as materials with a different refractive index and spectral dependence of it, the needed parameters for the design can be easily calculated [19].

Dielectric mirrors are composed of several thin dielectric layers. While they contain very thin layers of a mateiral with a high refractive index, also thicker layers with a lower refractive index are part of the mirrors. This yields a hig reflectivity at several surfaces, maximizing the overall reflectivity of the mirrors. They can be optimized for different wavelengths. Metallic mirrors however, have only one reflective layer, decreasing dispersion but at the same time also reflectivity. They are also not specially designed for certain wavelengths as dielectric mirrors often are, but support a broader bandwidth. In ultrafast applications, silver mirrors are hence preferable in order to keep the pulse short and not being bandwidth limited. One has to pay attention though at the damage treshold which is often much higher for dielectric mirrors.

2.4. Prism compressor

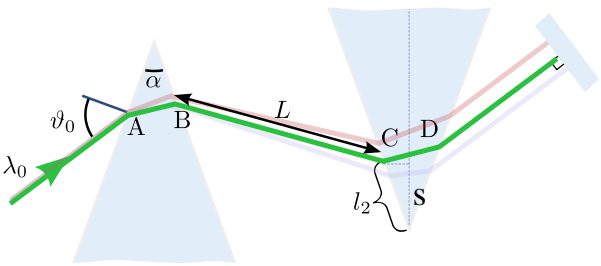

Figure 5: Schematic setup of a prism compressor. The traversed distance in the material has been changed in this experiment with the insertion S of the second prism.

In order to compensate the phase effects, mainly the second order, different compression techniques like grating compressors [20], chirped mirrors and prism compressors [21] have evolved over the years. The latter of the three has been employed in this experiment. The general principle can be explained as follows and is depicted in Fig. 5. The beam traverses the prisms one time along the green path and reflects back through the two prisms along the red path.

The prism splits several wavelenghts differently due to the angle of incidence

according to Snells law. Thus, the wavelengths arriving at the same angle of incidence exit the prism at different angles. Subsequently, the different wavelengths take different paths with varying length, such that when a second prism recollects the different wavelengths and parallelizes them again, all wavelengths arrive at the same time, hence maximizing the compression of the pulse.
This has been derived quantitatively in many standard textbooks, e.g., [22]. The second order phase contribution of a prism compressor then reads

$$\left.\frac{\mathrm{d}^2\varphi}{\mathrm{d}\omega^2}\right|_{\omega_0} = \frac{{\lambda_0}^3}{2\pi c^2}\left[L_g \left.\frac{\mathrm{d}^2 n}{\mathrm{d}\lambda^2}\right|_{\lambda_0} - \left(4L + \frac{L_g}{n^3}\right)\left(\left.\frac{\mathrm{d}n}{\mathrm{d}\lambda}\right|_{\lambda_0}\right)^2\right], \tag{12}$$

where λ_0 denotes the carrier wavelength, c the speed of light, L the distance between the two prisms and L_g the distance of glass traversed by the pulse. The derivations of the refractive index in terms of λ can be evaluated numerically by the Sellmeier equation with the respective coefficients for LAK-21 [23]. The exact third order contribution is somewhat more complicated if being represented in measurable variables[2]. As a thorough quantitative discussion of the TOD would be beyond the scope of this work, it is not given here.

For our experiment, we measured the insertion length of the prism S modulo a constant offset. As we were only interested in ΔS, this is of no further interest. The change of L_G can then be expressed as

$$\Delta L_G = 2\Delta S \cdot \tan(\alpha/2),$$

where $\alpha \approx 63°$ denots the apex angle of the prism. It can be determined from the fact that the prism compressor is placed in Brewster configuration and the resulting apex angle is $\alpha = 180° - 2\alpha_B$ with α_B being the Brewster angle.

The change in the GDD can then be modelled as

$$\Delta GDD(\Delta L_G) = \frac{{\lambda_l}^3}{2\pi c^2}\left[\left.\frac{\mathrm{d}^2 n}{\mathrm{d}\lambda^2}\right|_{\lambda_0} - \frac{1}{n^3}\left(\left.\frac{\mathrm{d}n}{\mathrm{d}\lambda}\right|_{\lambda_0}\right)^2\right] \cdot \Delta L_G,$$

As we hence expect have a linear dependence between ΔL_g and ΔS, the change in GDD is linear in the prism insertion length. The change in length l_2 from Fig. 5, which is essential for conversion from the simulation tools introduced in section 4.1, is given by

$$\Delta S = \Delta l_2 \cos(\alpha/2).$$

[2] Although a general form is given in [21], a more convenient, but larger expression has been derived in [24].

3. Methods and experimental setup

3.1. Temporal characterization of ultrashort pulses

While a spatial characterization of the beam using, e.g, a beam profiler mainly consisting of a CCD which records the intensity distribution of the beam, is relatively simple, techniques to characterize ultrashort pulses temporally are somewhat more sophisticated. This is the case, because in the general conception of temporal measurements, we need a shorter event or at least an event as long as the event to be measured, to characterize it temporally. As electronics cannot resolve below the low nanosecond or high picosecond regime, femtosecond laser pulses have to be characterized differently.

There exist various techniques like FROG [25], GRENOUILLE [26] and SPIDER [27], to name the most typical ones beside autocorrelation. However, the latter has various disadvantages, that the spectral phase cannot be retrieved and that it only works for well known-pulse shapes, being the strongest ones.

3.1.1. Autocorrelation

There are three main autocorrelation techniques, namely field, interferometric and intensity autocorrelation. The first one is of the form [19, p.880]

$$A(\tau) = \int_{-\infty}^{\infty} E(t)E^*(t-\tau)\mathrm{d}t, \tag{13}$$

and can be retrieved by using a Michelson interferometer with one interferometer arm delaying the pulse by a time τ, (Fig. 6 without Lens, SHG Crystal and Filter) which yields

$$I_M(\tau) = \int_{-\infty}^{\infty} |E(t) + E(t-\tau)|^2\mathrm{d}t, \tag{14}$$

containing the term $A(\tau)$ as seen by expanding.

However, to retrieve the temporal pulse envelope, we need a second order autocorrelator, e.g., the interferometric autocorrelator whose schematic setup is depicted in Fig. 6. Nonetheless, this yields a very complicated signal and the essential information about the pulse duration is difficult to extract. An easier determination of the pulse duration can be achieved using the intensity autocorrelation given by [28]

$$A(\tau) = \int_{-\infty}^{\infty} |E(t)E(t-\tau)|^2\mathrm{d}t. \tag{15}$$

This is more difficult to realize experimentally and is normally done as follows: The setup uses a non-collinear geometry in which the delayed pulse are focussed under different angles into the second harmonic generation (SHG) crystal, similar to Fig. 7. The beam

on the optical axis is extracted, because it is proportional to $E(t)E(t-\tau)$. By knowing pulse shape dependent numeric parameters, one can extract the pulse duration from this setup when the intensity autocorrelation is measured for several delays τ. [28]

As both methods do not allow us to measure the phase of the ultrashort pulse, different pulse measurement techniques have evolved over the years.

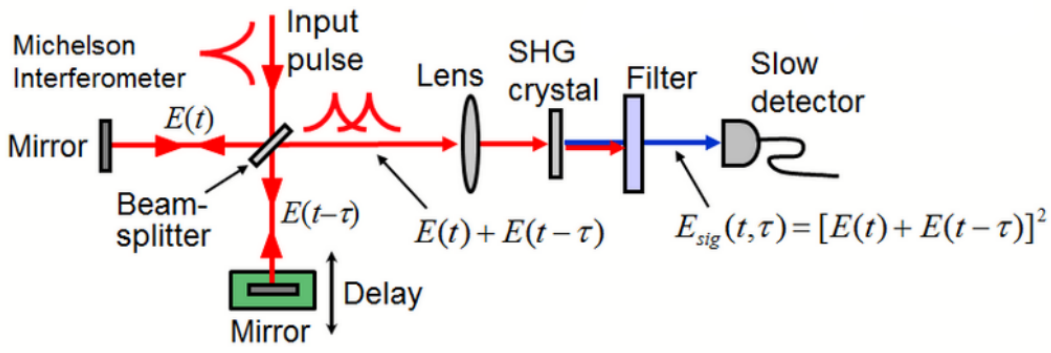

Figure 6: Schematic setup of an interferometric autocorrelator [29]. For intensity autocorrelation, the delayed pulses ae focussed under different angles into the SHG crystal and only the signal along the optical axis is extracted. For field autocorrelation, the detector is placed directly after the two pulses interfere, without focussing or SHG.

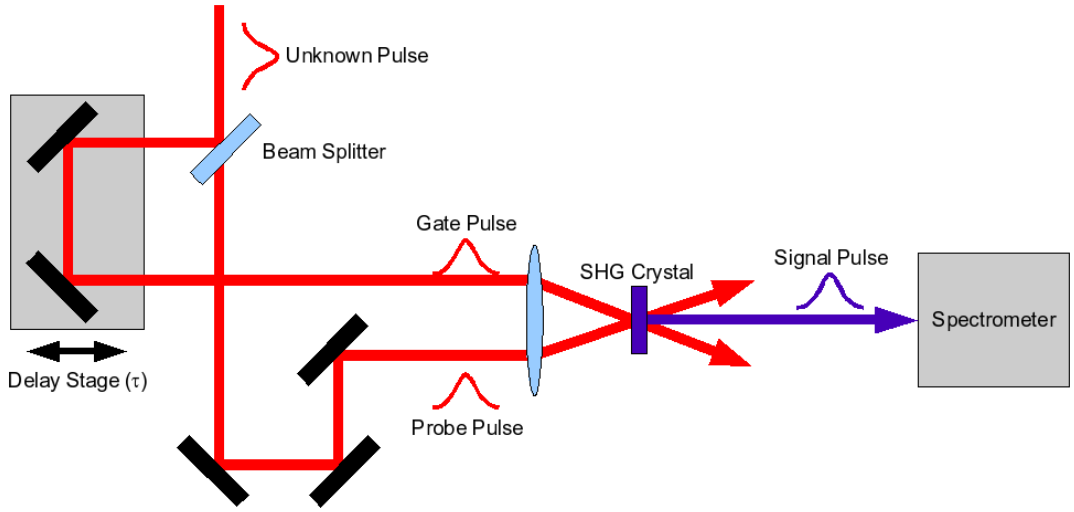

Figure 7: Schematic SHG FROG setup used for characterization of ultrashort pulses as taken from [30]. It only differs from an intensity autocorrelation by the spectrometers instead of a powermeters as a measuring device.

3.1.2. FROG

The first technique to solve the issue of reliable phase retrieval is *frequency-resolved optical gating* (FROG), introduced by Trebino *et al.* in 1991 [25], whose general setup is depicted in Fig. 7.

It is very similar to intensity autocorrelation, as essentially the whole setup, including the interferometer and SHG crystal is the same, except for the measurement device. Instead of a sole intensity measurement, the spectral intensity distribution is measured using a spectrometer. The FROG intensity is then given by [31]

$$I_{FROG}(\omega,\tau) = [\mathcal{FT}[E_{sig}(t,\tau)]^2 = \left|\int_{-\infty}^{\infty} E(t)E_{gate}(t-\tau)e^{-i\omega t}\mathrm{d}t\right|^2, \tag{16}$$

where $E_{sig}(t,\tau) = E(t)E_{gate}(t-\tau)$.

The exact form of the gate field E_{gate} depends on the FROG technique used, the most common gate is the SHG, where the gate field is exactly the electric field. The spectrum recorded for different temporal delays then yields the so-called FROG trace, from which the phase can be retrieved by a sophisticated algorithm. However, as noted in [32], the SHG FROG has an ambiguity in the sign of the spectral phase, thus the difference between positive and negative GDD cannot be extracted. This problem does not occur for different FROG techniques, e.g., a polarization based third order FROG.

3.1.3. GRENOUILLE

A somewhat simpler method based on FROG is *Grating-eliminated no-nonsense observation of ultrafast incident laser light e-fields* (GRENOUILLE). As seen in Fig. 8, it uses a horizontal cylindrical lens to generate a range of crystal incident angles, a Fresnel Biprism to split the beam into two parts which are subsequently suprimposed inside the SHG crystal, which is thicker than the normal one used in FROG.

The beam splits up in the biprism, and the respective parts have a delay along the horizontal direction, thus mapping temporal delay onto horizontal position. Moreover, the thick SHG crystal yields a limited phase-matching, dependent on the vertical angle of incidence, which has been varied using the horizontal cylindrical lens and thus also acts as a spectrometer. Phase-matching for second harmonic generation is an abundant topic and will not be further discussed here. The basic mechanism used however, can be summarized with the result that different fundamental wavelengths contribute to the upconversion process for different angle of incidence. As the frequency is doubled in the SHG, the resulting wavelength thus differs and angle of incidence and hence vertical position are mapped onto a spectral axis. After the SHG crystal, using a set of vertical and horizontal cylindrical lenses, we eventually obtain an image on the CCD which has a vertical wavelength and a horizontal delay axis. [26]

The GRENOUILLE technique has a further advantage: It can measure both spatial chirp and pulse-front tilt, which are inherently contained in the GRENOUILLE trace

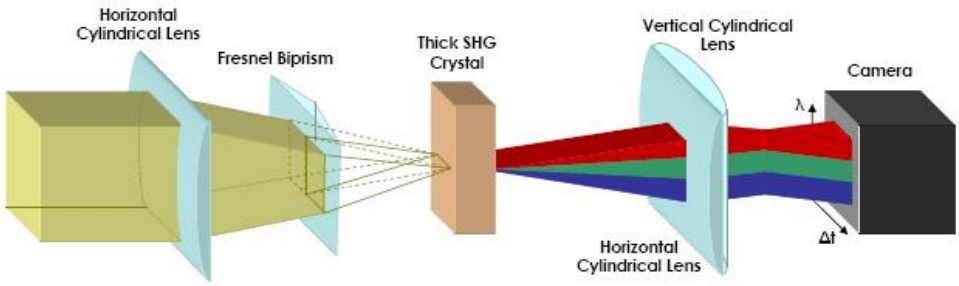

Figure 8: Schematic GRENOUILLE setup used for characterization of ultrashort pulses, taken from [33].

[31, 26]. Spatial chirp is indicated in the GRENOUILLE trace by a tilt of the otherwise symmetric trace. The pulse-front tilt can be registered as an off-center trace. This is well explained in Fig. 9(a) and Fig. 9(b).

The spatially chirped pulse has a non-symmetric overlap of the frequencies when being focussed into the SHG crystal, wherefore the GRENOUILLE trace tilts. As being elaboratly described in [31], the delay between the pulses is mapped onto position via $\tau = \alpha x$, with $\alpha = 2\sin(\theta/2)/c$. A linear spatial chirp[3] can be introduced by $\omega(x) = \omega_0 + \xi x$. The pulse with spatial chirp then yields

$$I_{FROG}^{SHG,chirp}(\omega) = I_{FROG}^{SHG}(\omega - 2\xi x, \alpha x)$$

as intensity. The slope of the GRENOUILLE trace is then $2\xi/\cos(\theta/2)$, thus by determining the slope of the tilted GRENOUILLE trace and removing the tilt, the FROG algorithm can be applied and the respective spatial chirp can be added again to the pulse afterwards. It is however important to note that the spatial chirp will eventually reduce the spectral bandwidth and hence lengthen the pulse duration.

In the case of a pulse-front tilt, the relative delay is shifted outwards which then yields the off-center trace. It cannot be measured in a classical one-shot SHG FROG setup, but in a GRENOUILLE setup, as instead of using a beam splitter, the beam is split in two halves from the center. The additional delay of τ_0 and $-\tau_0$ which is introduced on the respective parts of the beam, then yields the measured trace [26]

$$I_{SHG}^{GRENOUILLE,chirp}(\omega, \tau) = I_{SHG}^{FROG}(\omega, \tau + 2\tau_0).$$

The position dependent time is given by $t(x) = \zeta x$, where the parameter ζ can be extracted from $\zeta = \Delta x/(Lc)$ with Δx being the shift of the trace center and L the separation length between Fresnel biprism and SHG crystal.

[3]Higher orders are so far, to the best of our knowledge, not resolvable.

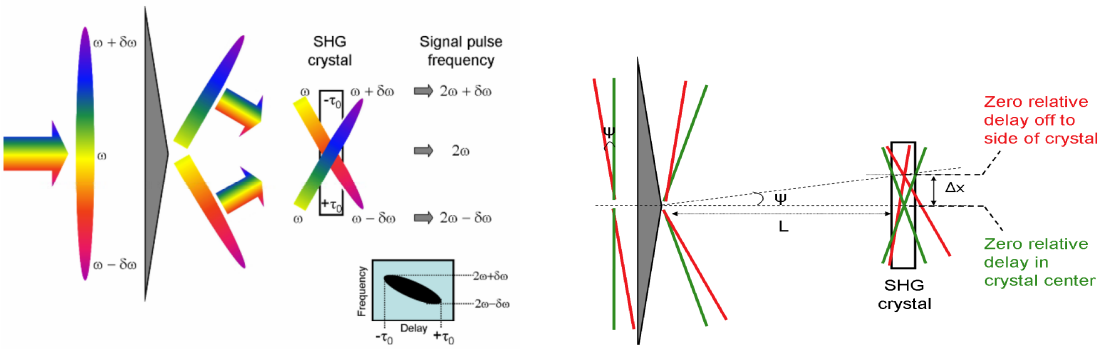

(a) Spatial chirp [31]

(b) Pulse-front tilt [26]

Figure 9: Spatial chirp and pulse-front tilt and its effects on the GRENOUILLE signal. The spatial chirp leads to a tilted trace, while the pulse-front tilt leads to an off-center shift of the trace.

3.2. Experimental setup

The main part of the experimental setup is formed by the 800 nm femtosecond laser (Tsunami, Spectra Physics) with an average power of 400 mW, a repetition rate of 76 MHz and a pulse duration of 22 fs at 58 nm bandwidth, although the bandwidth and thus the pulse duration can be tuned between 40 nm and 60 nm [34]. Along the beampath, a $\lambda/2$-waveplate which switches the polarization of the beam from s- to p-polarized, a prism compressor for reducing the GVD of the pulse and another $\lambda/2$-waveplate to switch the polarization back and attenuate the beam are placed in front of the GRENOUILLE apparatus (Swamp Optics).

For the prism compressor, an apex distance of 43.6 cm has been measured. The insertion length of the second of prism can be changed paralellel to the apex using a micrometer screw.

The GRENOUILLE is directly connected to a computer and can be controlled via the QuickFrog Software (Swamp Optics). The space mode allows for aligning the beam into the GRENOUILLE, while the time mode provides the user with spectral and temporal reconstruction of the pulse including amplitude and phase.

Besides the main elements mentioned above, several BK7 windows, a MgF_2 wedge and MgF_2 lenses, a chirped mirror pair and a long-/shortpass filter are avalaible to be placed in the beampath. Moreover, either dielectric or silver mirrors can be used in the experiment, by switching beam paths using flippable mirrors. As the schematic setup does not change in this case, only two beam paths are depicted in Fig. 10.

At first, beam path 1 in Fig. 10(a) is aligned and the influence of the position of the second prism of the prisms compressor on the pulses properties is studied in order to find the optimum position. Subsequently, the elements listed above are added to the

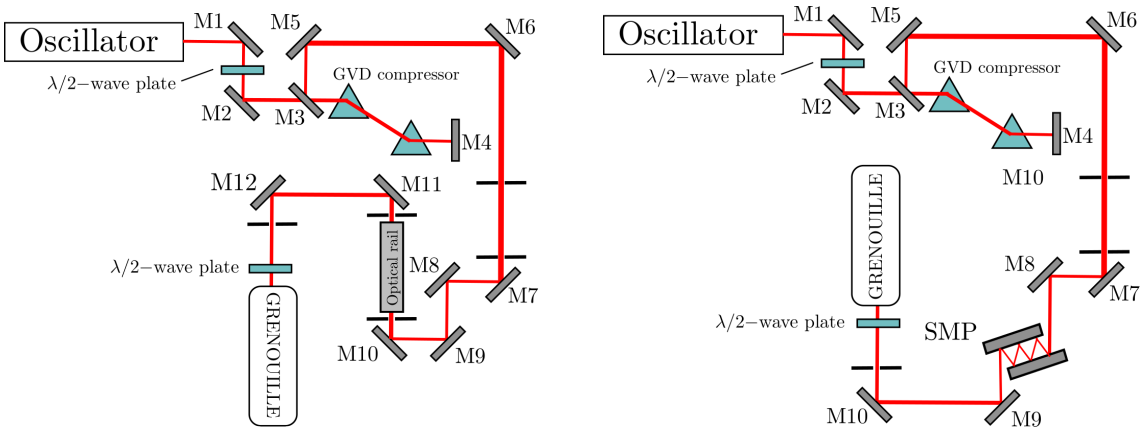

(a) Path 1,2 (b) Path 3

Figure 10: Schematic experimental setup for the different beampaths, the respective optical elements are added in beam path 1 on the optical rail.

beampath at the position of the optical rail and data is recorded before material insertion as well as before and after phase compensation by adjusting the prism compressor. For one BK7 element, the glass is tilted by about 45° and subsequently replaced by a BK7 wedge with an opening angle of 6°. At last, the effect of a MgF_2 lens telescope on the beam and pulse properties are examined. The second beampath is only a slight variation of the first beampath, only M7-M10 are replaced by dielectric instead of silver mirrors. For the square mirrors (DCMP175 from Thorlabs Inc.), the setup is slightly changed to beam path 3 (see Fig. 10(b)). It is important to note that before each experiment, the prism compressor is set back to optimum position. As the second beampath yielded extremely distorted pulses, such that a reconstruction from the retrieved FROG trace has not been possible, the same beampath has been used at a lower laser bandwidth of 36 nm.

4. Measurements and Analysis

In the following, the experimental results should be discussed. Only the change in the insertion length of the prism has been recorded analogously, while all other data has been directtly recorded by the QuickFrog software. At first, the GDD of the pulse has been measured for different prism insertion lengths such that a quantity for the added GDD per inserted mm can be derived and used later one. Subsequently, the GVD of different materials can be measured by simply placing them along the beam path. The effect of tilted glass plates and a wedge as well as a lens telescope on the pulse-front tilt and spatial chirp is further examined. Moreover, the spectral and temporal effect of a long- and a shortpass is studied. At last, this work will discuss the influence of dielectric vs. silver mirrors and chirped mirrors on spectrum and spectral phase.

Unfortunately, we assume to have made several errors while recording the experimental data which can be partially corrected. Which values have been corrected and for which reason will be thouroughly explained in order to sustain scientific working standards in appendix A.

4.1. Prism compressor

At first, the pulse measurement conducted with the GRENOUILLE has been performed for multiple insertion lengths of the second prism of the prism compressor. By employing a phase fit up to the third order, the GDD and TOD of the respective pulses can be determined. The measured GDD as a function of prism insertion length is plotted in Fig. 11(a) as well as the resulting pulse duration. The sign of the GDD has been corrected according to the expected behavior from the theoretical calculations[4], for more on this see appendix A. The lenght l_2 in Fig. 5 has not been measured and thus we cannot evaluate a constant offset of the measured GDD, exacerbating comparing the theoretical to the experimental results. However, as we expect a linear dependence on the insertion length as explained in section 2.4, we can compare the slope.
Hence, we applied a linear regression to the experimental data and obtained a slope of $(189 \pm 27)\,\mathrm{fs}^2/\mathrm{mm}$. The theoretical simulation yields slightly different results, depending on which method (own simulation, vChirp Software (Laser Quantum) or Optics Toolbox from Light Conversion[5]) has been used, but are either $150\,\mathrm{fs}^2/\mathrm{mm}$ or $155\,\mathrm{fs}^2/\mathrm{mm}$. The respective values together with the percentage deviation of the experimental data are shown in table 1.
The deviation between simulation and experiment is large, no matter which method is used. Even the agreement between the linear regression and the data points is detoriated by the two deviating data points for an insertion length of 27 mm and 27.26 mm. Furthermore, the slope for high and low insertion length seems to differ, as it seems

[4]Thus, a higher GDD from a larger insertion length of the prism.
[5]`http://toolbox.lightcon.com/tools/prismpair/`

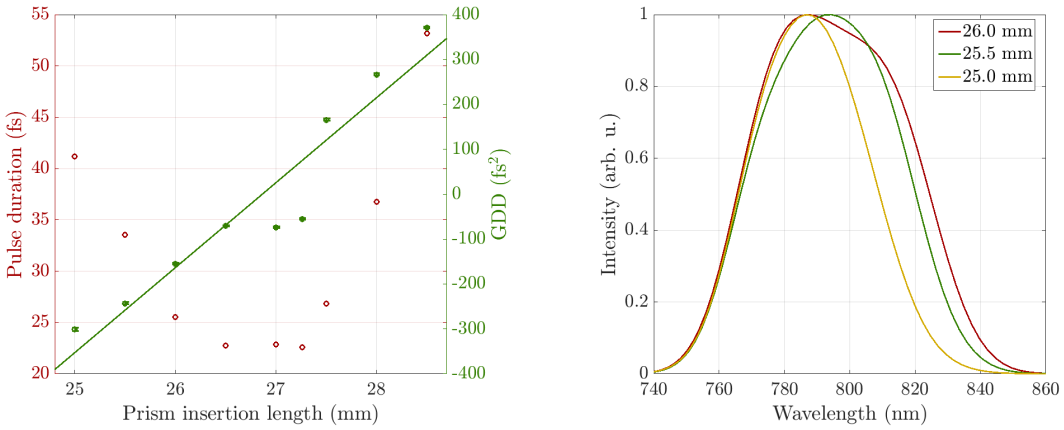

(a) Pulse duration and GDD

(b) Bandwidth

Figure 11: Experimental result for GDD and pulse duration for different insertion length of the second prism in the prism compressor (a). The slope of the linear regression is $(189 \pm 24)\,\mathrm{fs}^2/\mathrm{mm}$ In (b) the bandwidth dependency on the prism insertion length is plotted.

	Fit	Theory	Toolbox	vChirp
GDD/mm (fs^2/mm)	189 ± 27	150	155	150
Deviation (%)		19 ± 11	17 ± 11	20 ± 11

Table 1: Simulated results for the GDD/mm of the prism compressor dependent on Δl_2. The value under "Theory "has been simulated as explained in section 2.4.

less steep for lower insertion lengths. Although we cannot fully assume the prism compressor to function as expected, we believe that rather the GRENOUILLE does not provide reliable results. For the deviation of the single data points, several reasons, from erronous read out from the micrometer screw to a simple measurement error in the GRENOUILLE, can be suspected. In this context, it is important to mention that while the FROG error was small, the QuickFrog program used to decrease the sample rate of the GRENOUILLE trace[6], presumably in oder to guarantee live-reconstruction. However, this can substantially reduce the accuracy of the reconstruction and yield this large deviations.

It is surprising, that the GDD behavior is is still linear for small prism insertion lengths. As seen in Fig. 11(b) the bandwidth is substantially reduced in case of clipping the beam. This can be easily understood as follows: As the wavelengths get spatially separated by the first prism, the part of the beam cut at the apex corresponds to a clipping of wavelengths on the low wavelength part of the spectrum. The corresponding bandwidth dropped from 56-59 nm down to 43 nm. Nevertheless, we were not able to

[6]This will be further discussed later.

finally explain why the GRENOUILLE monitors a cutting of the spectrum on the high wavelength instead of the low wavelength edge. If further studied, detailled examination of the spectrum inside the prism compressor would be inevitable. Assuming, that this clipping is nonetheless real and not a measurement artefact, we can conclude that it does not seem to influence the spectral phase, but obviously the pulse duration via equation (12). This could also explain, why the pulse duration for a similar absolute value of the GDD is larger for a negative prism insertion length. One can make sense of this result by assuming that the clipping does not yield any interference patterns on the beam profile. In this case, just a part of the spectrum misses, thus part of the amplitude is equal to zero, but the phase can be seperated from this and is still the same along the remaining spectrum.

Generally, the evident and expected connection between GDD and pulse duration can be seen in Fig. 11(a). As the GDD decreases, but increases in its absolute value, the pulse duration increases notably, as expected after equation (7). It is easily observable, that an optimum position can be found around an insertion length of 27 mm. It was difficult to tune for the exact lowest pulse duration in the experiment, thus the optimum position varied slightly for every experiment. The clipping of the beam described above can apparently be traced back to a suboptimal alignment of the prism compressor and reduces it's operational range. This is especially relevant for the experiments performed later on, where the insertion of dispersive material cannot be fully compensated.

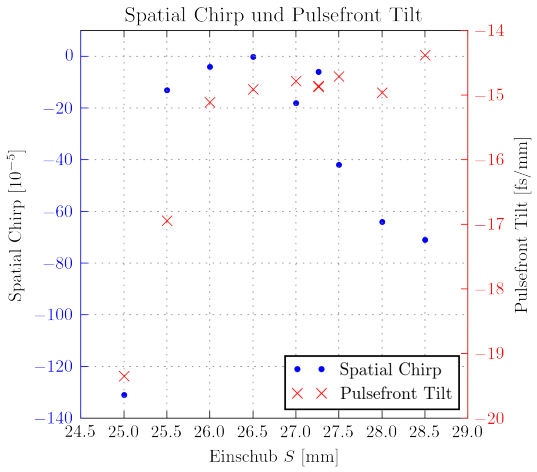

Figure 12: Spatial chirp and pulse-front tilt caused by the prism compressor as a function of the prism insertion length (Einschub S).

Another issue and a very important one to study, control and monitor is the spatial chirp and pulse-front tilt caused by the prism compressor itself. Although both should not be present in a perfectly aligned prism compressor, those effects are very likely to occur. In Fig. 12, the pulse-front tilt and spatial chirp are plotted as a function of the prism insertion length. First regarding the spatial chirp, it is apparent that it substantially varies for different insertion lengths. As seen in the evaluation of the experiments with tilted BK7 plates, the spatial chirp caused by the prism compressor is larger than the one intentionally caused in the experiment. Especially for small insertion lengths, the spatial chirp increases in value and presumably occurs due to clipping on the apex of the prism. The change for higher insertion lengths could possibly be explained with a misalignment of the prism compressor as discussed in section 2.2.1 Moreover, the pulse-front tilt shows a somewhat similar behavior. It is approxi-

mately constant for most of the insertion lengths but also drops severely for low insertion lengths. The figure can be used to show quantitatively, that the prism compressor is not well-aligned and distorts the pulses spatially.

4.2. Glass insertion

In the following part of the experiment, 5 mm, 10 mm, 15 mm of BK7 and 5 mm of MgF_2 have been inserted into the beampath. The obtained values for the GDD are listed in table 2. As the dispersive effects of BK7 and MgF_2 are well known by their Sellmeier equation, the expected GDD can be compared to the theoretical results. The compensation column gives the values which we calculated from the change in the insertion length of the prism together with the slope of the linear regression from above. In order to clarify the effect of GDD on the pulse duration, the resulting pulse durations are also given in table 2.

As mentioned previously, the GRENOUILLE cannot discriminate between positive and negative GDD, wherefore the signs in this part of the experiment have been chosen such that a realistic value can be obtained and, as the initial position of the prism compressor remained approximately unchanged, the initial GDD has been chosen to be always negative. Nonetheless, the phases plotted in Fig. 13 have been unchanged in order to underscore the contrast between the results in table 2 and the actual measurement. The phases for the tilted BK7 plates are not shown and just given as an additional value in the table, because we do not know the exact tilting angle which is why the focus should not remain on this two measurements.
In order to underscore the effects of compensation by the prism compressor, the phase before material insertion, after material insertion and after compensation are plotted in Fig. 13.

From Fig. 13 it is directly apparent that the exact influence of the material can only be extracted if it is at least partially known, which is suboptimal for an experiment. In case of assuming the theoretical values or at least their order of magnitude and sign, one can obtain results varying in reliability. While 10 mm and 15 mm of BK7 yield experimental values relatively close to the theoretical expectation, the deviation for 5 mm of BK7 and MgF_2 respectively, is large. Especially for the latter one, this might be caused by a generally small GDD added to the pulse wherefore smallest deviations in GRENOUILLE alignment yielding a slightly different result affect the measurement substantially. The absolute deviation for 5 mm and 10 mm of BK7 are comparable, thus if assuming a general error of around 50 fs^2 of the GRENOUILLE, the deviations could be explained. As 50 fs^2 translate into several femtoseconds difference for a 20 fs Fourier limited pulse, this error is not acceptable. If provided with more time, it might have been reduced by carefully realigning and optimizing the alignment of the GRENOUILLE. Moreover, it could occur due to the undersampling[7] by the QuickFrog software used for

[7] See section 4.7.

		Induced GDD	Theory GDD(GVD)	Compensated GDD	Theory GDD(S)	initial	without compensation	with compensation
BK7	5 mm	271 ± 3	223	-283 ± 3	-257 ± 34	22.4	31	23
	10 mm	482 ± 4	447	-552 ± 3	-513 ± 96	22.10	65.60	27.20
	15 mm	666 ± 4	670			21.90	99.90	
	tilted 45°, 5 mm	264 ± 3	316	-291 ± 3	-251 ± 34	22.40	31.60	23.40
	tilted -45°, 5 mm	300 ± 3	316	-321 ± 3	-277 ± 37	22.70	34.80	23.50
MgF2	5 mm	139 ± 4	100	-142 ± 3	-164 ± 22	22.20	23.60	22.40
	Thickness	GDD (fs^2)				Pulse duration (fs)		

Table 2: Measured and theoretical expected GDD added by different dispersive materials with different thicknesses. The theoretical value GDD(GVD) has been calculated from the Sellmeier equation given by [23], [35]. Theory GDD(s) has been calculated from the known change in the insertion length of the prism together with the result from the linear regression above. Note, that compression for 15 mm of BK7 has not been possible with the prism compressor without substantial clipping of the beam/spectrum.

accelerating the reconstruction algorithm. Errors like a varying thickness of the glass or a slight tilting ($\pm 3°$) when placing it on the optical table can be precluded because both effects would not add or substract any GDD larger than $5\,fs^2$ [36]. For the tilted windows, another error caused can be the inaccuracy of the tilting angle. It is hence not surprising that the GDD values differ again from the theoretically expected values.

In the case of 5 mm of BK7, the compressed phase looks similar to the phase before material insertion, but the GDD has been slightly overcompensated. However it is apparent that the influence of such a BK7 plate can be neglected in experimental application, when being compensated by a prism compressor. For 10 mm plate thickness, the compressed phase shows a non negligible amount of negative GDD[8]. The limited compressability can be traced back to the clipping of the beam at the apex of the prism, as mentioned previously, which limits the amount of compensable GDD and the bandwidth. In this case, we chose to minimize the pulse duration, not the GDD, which being combined lead to the optimum position to be overcompensating the GDD. It is also possible that we simply did not optimize the pulse duration properly. However,

[8]Although a positive GDD might be more intuitive, we extrincated the prism by such a large amount that the GDD must be negative according to the previous evaluation of the prism compressor.

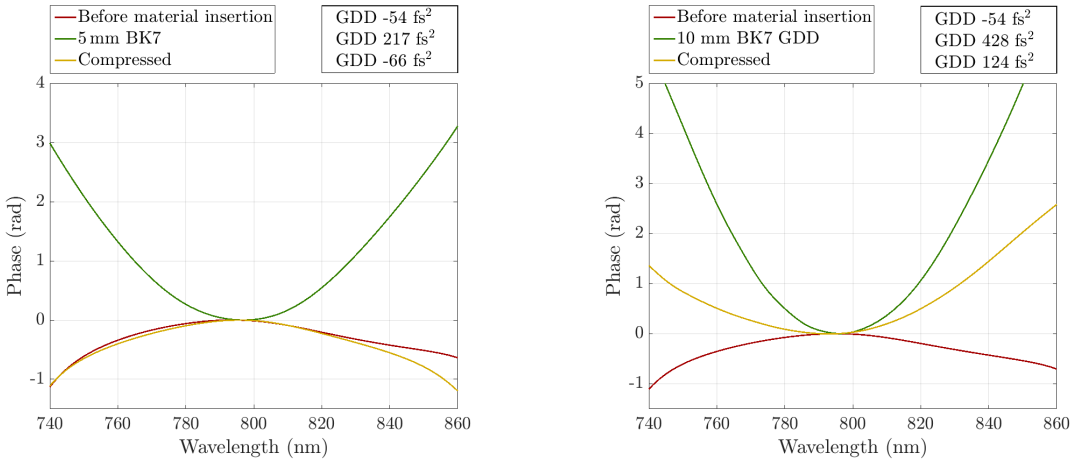

(a) 5 mm BK7

(b) 10 mm BK7

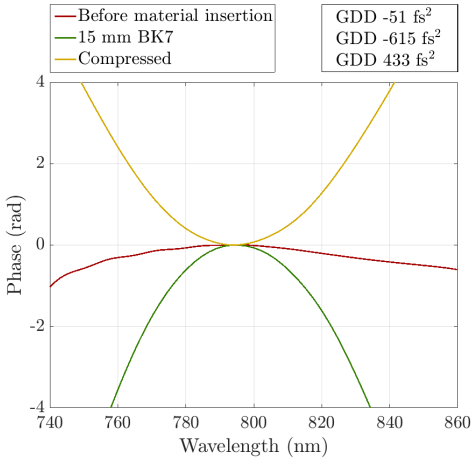

(c) 15 mm BK7

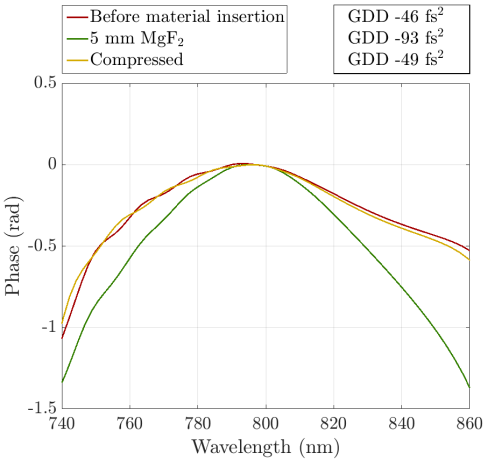

(d) 5 mm MgF_2

Figure 13: Measured spectral phases before material insertion, with different inserted materials and after compression.

the compensated GDD is with deviations below 30 fs^2 from the measured induced GDD, generally relatively precise. This holds not true for 10 mm of BK7, as discussed previously. Generally, higher orders, e.g., TOD, can be partially compensated or added by the prism compressor if its is not optimally aligned, which eventually may yield a compression or streching of the the pulse when trying to compensate GDD only. In our case we expect higher orders to become stronger as the initial pulse duration can never be reached again. It can though not be ultimately said if this arises from the prism compressor or the higher orders of the inserted materials.

The measured compensated GDD is still in the uncertainty range of the theoretical calculated one. This is however no surprise as the errors are simply large. The deviation

is the largest for the tilted BK7 plates which can again be traced back to non precise tilting and other effects like spatial chirp which can change the local bandwidth of the pulse and thus change how it can be optimally compressed. For 15 mm thickness, no real compression has been possible due to the bandwidth losses when further moving the prism outside the beam.

Another effect which should have been observable is that the TOD is not compensable with the prism compressor. Even more, it can arise from the prisms compressor if the angles of the two prisms deviate from their optimal position by only a small extent. However, the TOD wildly fluctuates between positive and negative values and shows no clear tendency. Further analysis is exacerbated by the fact that we again have an ambiguity towards the sign of the spectral phase. It can neither be precluded that the prism compressor adds TOD, nor that it does not. Furthermore, although BK7 as well as MgF_2 should add a positive amount of TOD according to their Sellmeier equation, there is no clear tendency for these materials either. This might again be caused by the ambiguity of the sign of the spectral phase.

4.3. Pulse-front tilt and spatial chirp

One BK7 plate is subsequently tilted by approximately 45° in both left and right direction. Moreover, after the plate has been removed, a BK7 wedge with an opening angle of approximately 6° is placed inside the beam path. The latter one has been added after building a 1:2 telescope with MgF_2 lenses discussed in the next section. The effect to study is no more the sole GDD, but much more the spatial chirp added to the pulse. The QuickFrog (Swamp Optics) software inherently provides a value for the spatial chirp and pulse-front tilt, wherefore the scheme described in section 3.1.3 has not been applied to the retrieved FROG traces. The theoretical value of 5.6 fs/mm for the pulse-front tilt has been calculated according to section 2.2.2.

4.3.1. Spatial chirp

From table 3, one notes the following about the influence of material insertion and prism compressor on the spatial chirp and pulse-front tilt.

First of all, the material insertion always yields a negative spatial chirp, despite different tilting directions, although we would expect a different sign for a right- and a left-tilted Bk7 plate. Moreover, the spatial chirp for the untilted BK7 is surprisingly large, although we would expect no spatial chirp at all if the window is not tilted. The deviation, also for different tilting angles, can be partially explained with the inaccuracy when tilting. This can also be seen from table 2, where we observe a difference in the induced GDD. For the wedge, the change in spatial chirp is the largest. As we did not measure which thickness the wedge had at the point where the beam traversed it, this might simply result from a different thickness in addition to the angular dispersion arising from its prism-like structure.

Object	Spatial Chirp $[10^{-5}\Delta\lambda/\Delta x]$		PFT [fs/mm]	
	no Comp.	w. Comp.	no Comp.	w. Comp.
5 mm BK7	-35	-11	0.64	-0.67
45° 5 mm BK7	-22	-32	3.95	2.87
-45° 5 mm BK7	-35	44	-3.12	-4.75
Telescope MgF2	-9	-3	0.48	-0.94
6° Bk7 Wedge	-55	-38	8.1	7.43
6° Wedge(theo.) BK7			5.6	

Table 3: Measured difference in spatial chirp and pulse-front tilt (PFT) when adding different objects to the beam path. Wihtout is abbreviated by w., compensation by Comp. The theoretical value for the pulse-front tilt has been calculated according to section 2.2.2. A typical initial spatial chirp is in the order of $-6 \cdot 10^{-5}$, an initial pulse-front tilt around -14.87 fs/mm, both has been reproducable.

Secondly, the prism compressor seems to influence the spatial chirp, it is unclear though in which direction, as it seems to decrease when compensating with the prism compressor (extricating the second prism), except for the right tilted wedge, although the prism has always been moved in the same direction. From Fig. 12 we would rather expect always a decreasing spatial chirp when extricating the prism. Even more, the strong deviations not only in the qualitative behavior (larger or smaller spatial chirp), but also in the quantitative behavior among all the values after compression are unexpected, as, the prism insertion length varied by maximally 0.1 mm for all values in the second column (w.Comp).

It is important to note in this context, that the sign for the (-45°)-tilted BK7 flips sign after compression. A possible explanation is the previous pulse being too long to fully retrieve an accurate spatial chirp quantity or simplay any other measurement error of the GRENOUILLE. As the sign-flip leaves us with the expected behavior, at least assumptions about possible flaws of the measurement without compensation are valid. However, the lack of lab-time did not allow us to further pursue the validation of this theory.

In this section, no theoretical values have been derived to which one could compare the measured ones. However, the tendency that the insertion of a tilted material or a wedge yields a spatial chirp, has been expected from section 3.1.3. As no experience values concerning the quality of the spatial chirp determination using the GRENOUILLE are known by us or any other member of the research group, we were not able to determine if the deviations are too small to be reliably measured or not. It is important to note that even the manufacturer of the GRENOUILLE device answered after several queries that the GRENOUILLE is not optimal for an accurate measurement of spatial chirp and suggested to use a spectrometer instead. It can though be noted that no sincere conclusions can be drawn from this experimental values.

4.3.2. Pulse-front tilt

In the optimum case, we would expect no pulse-front tilt at all from the glass, no matter if tilted or not. However it is clear from table 3, that we obtain a slight pulse-front tilt change from the untilted glass, but a much larger one from the tilted BK7. As explained in section 2.2.2, this behavior might arise from initial spatial chirp, however this does not explain why the pulse-front tilt is subtantially larger for the tilted glass plate[9]. Most notable, we obtain alternating signs depending on the tilting direction. Thus, when placing the right-tilted BK7 plate in the beampath, the pulse-front tilt is reduced, while it is increases by a comparable amount for the left-tilted BK7. Maybe, a combination of elicited additional spatial chirp which has a different sign depending on the tilting direction, subsequently yielding pulse-front tilt could explain this behavior, but this is rather a vague assumption to be further studied than a waterproof reason. Besides, the pulse-front tilt is substantially increased for the wedge, as it acts like a prism.

The prism compressor seems again to influence the pulse-front tilt and again not consistently. The order of magnitude of the changes is however in the range of the fluctuations observed in the evaluation of the prism compressor wherefore we hesitate to interpret too much into these experimental values.

The theoretical value has been calculated for a perpendicular incidence on the BK7 plate, as we were unsure at which tilting angle we placed the wedge inside the beampath. As the order of magnitude fits very well to the measured one (deviation $\approx 30\%$), we can at least assume that the measured signal was no noise, but evoked form the optical elements inside the beam path.

4.4. Lens telescope

When inserting the lens telescope into the beampath, it should be aligned such that no spatial chirp and no pulse-front tilt is induced. The respective values are shown for clarity in table 3.

From the experimental results no large effect on the spatial chirp can be seen, actually the values are the smallest for all inserted objects and can rather be traced back to smallest misalignment and general fluctuation of the measurements. As expected, the pulse-front tilt shows only minor fluctuations, smaller than for an inserted plate of BK7. It can thus be concluded that the telecope was relatively well aligned.

Another effect can be seen in the bandwidth of the ultrashort pulses. The initial bandwidth of 52.6 nm is reduced to 49.9 nm. There are two possible reasons for this effect. The first is that generally the bandwidth fluctuated when tuning the prism compressor, however, the respective insertion lengths were in a range where the bandwidth remained nearly constant and fluctuated less (± 0.5 nm) than the value indicated above.

It is therefore assumed that this change has to be caused by the lens telescope. Although not fully quantitatively elaborated in this work, the general principle might be

[9] As the traversed distance increases with $\sqrt{2}$ only a small change would have been expected.

understood as follows. As the refractive index differs for different wavelengths, the focii of different wavlength thus vary. This is known as chromatic aberration and leads to the situation that shorter wvelengths are focussed stronger. As a result, the telescope only collimates a certain part of the wavelengths, while others diverge along the beampath. As during the experiment there has been no time left to work with achromatic lenses, it can only be assumed that this issue might be solved by using achromatic lenses, which have been further described in 2.3.

Another possible explanation is that previous spatial chirp in combination with a non-perfectly aligned telescope lead to a slight divergence of the outer part of the beam which had a different wavelength constitution, thus effectively reducing the bandwidth arriving at the GRENOUILLE.

4.5. Long- and Shortpass

By adding either a longpass or a shortpass to beampath 1, the bandwidth of the ultrashort pulses can be substantially reduced above or below 800 nm. After equation 4, this should yield a longer pulse duration.

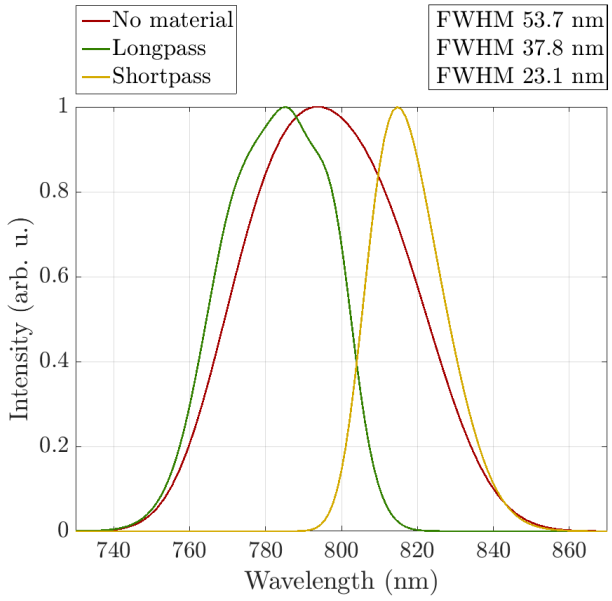

Figure 14: Different spectra for undistorted pulses as well as distorted pulses by placing either a longpass or a shortpass.

From the plotted spectra in Fig. 14 it can be observed that the expected effect indeed sets in, however interchanged, as the longpass should let long wavelengths pass and vice versa. For the longpass the spectral bandwidth is reduced by almost 30%, while it is even further reduced by 57% in the case of the shortpass. This large difference in bandwidth reduction can be traced back to the fact that the passes do not have sharp absorption edges, but rather a smooth transition.

Thus, it is possible that the shortpass simply cuts sharper than the longpass at the 800 nm edge. Moreover, the spectrum is generally centered around a central wavelength below 800 nm, which amplifies the observed effect. As mentioned previously, from the spectral change a different pulse duration is expected. This holds true, as the respective pulse durations are 22.3 fs (initial pulse), 52.8 fs (longpass) and 44.4 fs (shorpass). However, the longer pulse duration for the pulse passing through the longpass is surprising. It simply arises though due to a much larger GDD for the longpass. As we did not adjust the GDD, this effect can of course not be

precluded.

By regarding the Fourier limit, the phase influence can be excluded. In this case the pulse durations read 21.7 fs, 30.3 fs and 43.5 fs for the initial pulse, the long- and the shortpass respectively, thus prooving the general claim made in the theory.

As mentioned in the beginning, the long- and shortpass yield the exactly interchanged result as expected. As we do not assume a commercially available software to be such substantially flawed, we believe that either by fault of the experimentalists or the assistants who labelled the optics, the two optics have been mixed up. Important to mention is though that a mislabelling of the wavlength axis from the QuickFrog software could explain, why the wrong wavelengths are cutted inside the prism compressor as elaboratly discussed in section 4.1.

4.6. Dielectric mirrors

When changing the setup to beampath 2 (Fig. 10(a)), four of the silver mirrors have been replaced by dielectric mirrors, not further specified to be suitable for ultrashort laser pulses. As evident from Fig. 15, the retrieved frog trace is notably distorted and thus yields no meaningful electric field reconstruction of the pulse (not shown). This effect presumably occurs due to the fact that cheap dielectric mirrors, not optimized for employment together with ultrashort laser pulses, provide the pulses with a distorted phase profile, candidly speaking fully destroying the pulse. This proposition can be supported by examining the effects of the dielectric mirrors on pulses with a reduced bandwidth, with the results plotted in Fig. 16.

First of all, from Fig. 16(a), it can be observed that the spectrum underlies notable distortion after reflection from the dielectric mirrors. Several reasons might occur which lead to this behavior: One possible reason is a varying reflectance of the dielectric mirror which directly affects the observed spectrum. Even more, the phase shows a very large GDD. As the spectrum is narrower, although the GDD is large, it might still yield a resolvable pulse duration. The large negative GDD is apparent. However, we assume this GDD to be positive, as, as mentioned previously, the SHG GRENOUILLE cannot disciminate between positive and negative GDD. The difference between the retrieved and the experimental FROG trace are large as can be seen in Fig.17. Thus, the reconstructed spectrum, the reconstructed

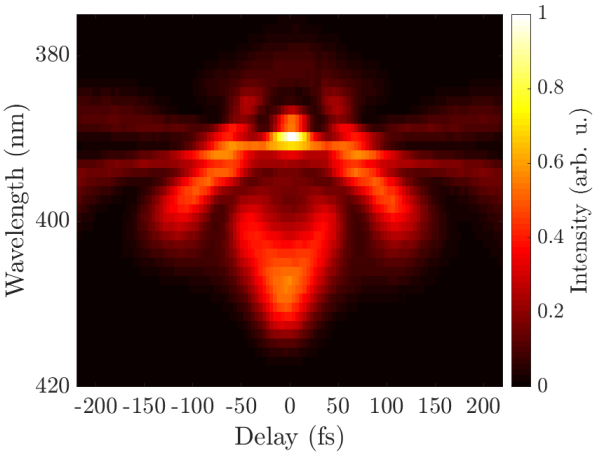

Figure 15: Retrieved FROG trace for beampath 2 with four dielectric mirrors instead of silver mirrors.

spectral phase and thus consequently the time domain reconstruction have to be regarded cautiously and cannot be assumed to describe the actual pulse.

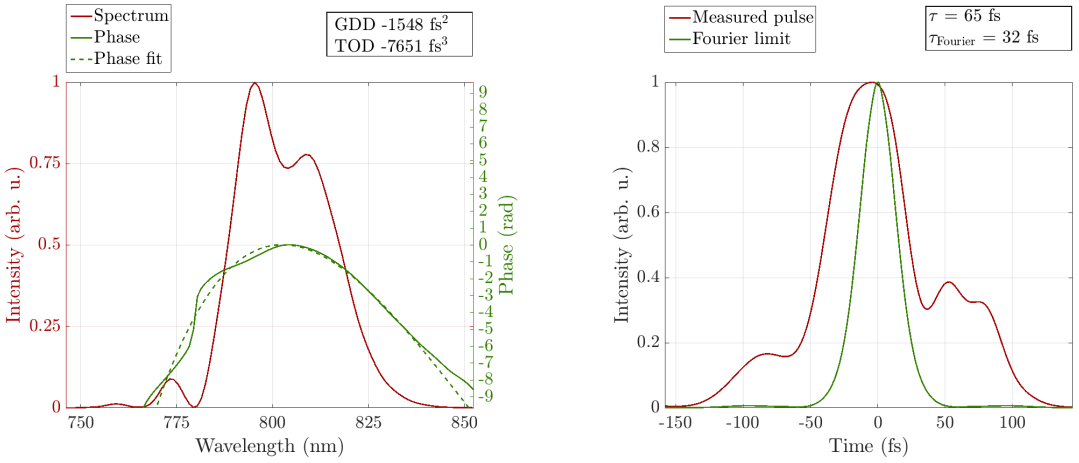

(a) Spectral domain (b) Temporal domain

Figure 16: Spectrum and spectral phase as well as reconstructed pulse and Fourier limited pulse for beampath 2 with a reduced bandwidth of 30 nm.

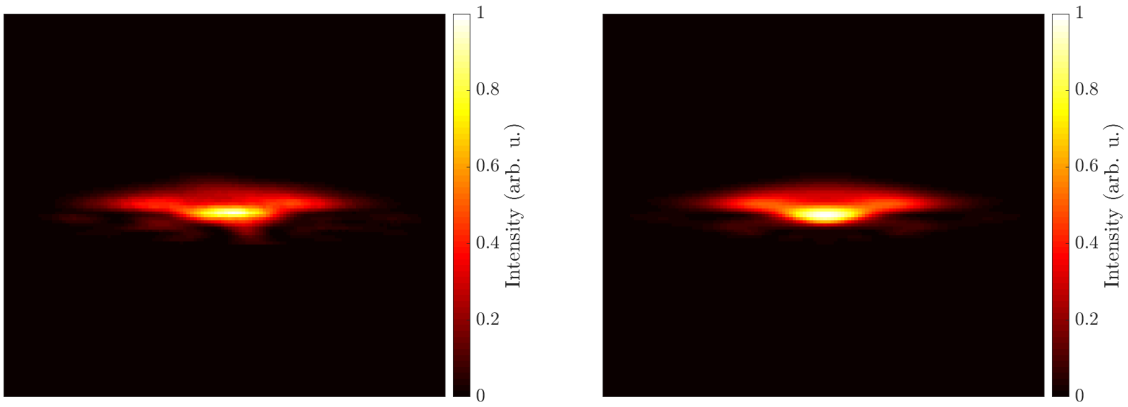

(a) Experimental (b) Retrieved

Figure 17: Experimentally measured and retrived FROG trace for the dielectric mirrors with the Tsunami emitting pulses with a smaller bandwidth.

The resulting temporal shape thus shows, non surprisingly, a large deviation from an ideal gaussian or sech^2 pulse. Although the FWHM pulse duration is about 65 fs, the pulse shows a broad pedestal for negative and positive times and thus will effectively act like a much longer pulse[10].

[10]Generally, the pulse duration definition in terms of the FWHM is no more meaningful fur such

4.7. Chirped mirrors

At last, the chirped mirrors should be characterized by their effect on the spectral phase and the pulse duration. From Fig. 18, one can again obtain that the spectrum seems to be distorted. This is surprising, as the mirrors have proven to be well suitable, spectrum and spectral phase wise, for comparable bandwidth and much higher intensities (1.9 mJ at 20 fs and 6 mm beam diameter) [37]. Besides the spectral change, the most apparent feature is the large amount of negative GDD added to the pulse. As the underlying chirped mirrors (DCMP 175, Thorlabs Inc.) add approximately 175 fs^2 per bounce [38], and 10 bounces have been performed on the chirped mirrors, this is not surprising. The prism compressor has been in optimum position previously (-50 fs^2), thus the determined GDD averages to 141.2 fs^2 per bounce on the chirped mirrors, deviating by approximately 20% from the theoretical value. Since the GDD is large, the measured pulse duration is with 179.3 fs also. However, still pedestals at a low intensity can be observed. As the Fourier limit provides a nearly gaussian temporal intensity, it can be assumed that the suboptimal pulse shape emerges from an interplay of large GDD and distorted spectrum. Again, it is inevitable to mention that different experiences have been presented in [37].

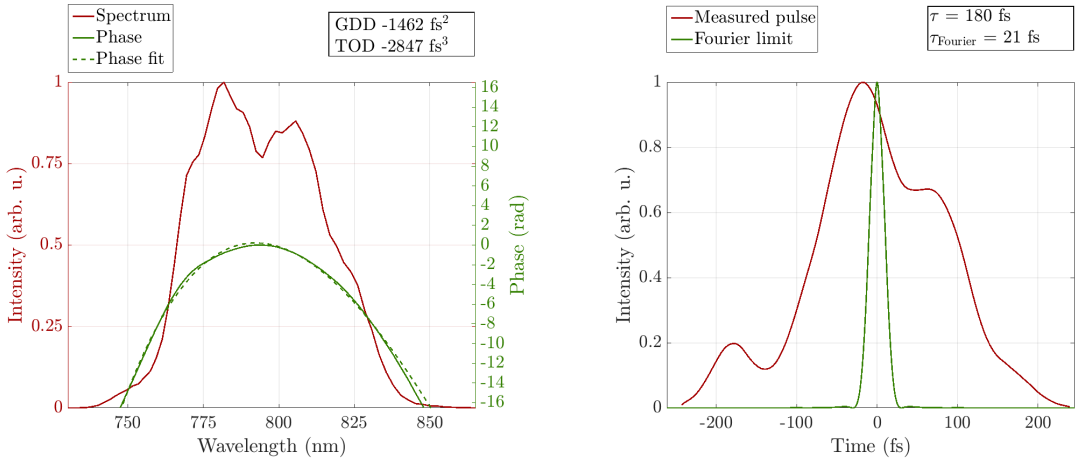

(a) Spectral domain

(b) Temporal domain

Figure 18: Spectrum and spectral phase as well as reconstructed pulse and Fourier limited pulse for beampath 3.

This might also be explained with the effect mentioned in the previous evaluation that the difference between the retrieved and the experimental FROG trace are large as can be seen in Fig.19(a) and 19(b). Thus, the reconstructed spectrum, the reconstructed spectral phase and thus consequently the time domain reconstruction have to be regarded cautiously and cannot be assumed to describe the actual pulse. Furthermore, the FROG trace is clipped, wherefore optimal reconstruction is hindered.

strongly distorted pulses.

One last, but important factor which has to be considered is the undersampling of the QuickFrog software which obviously affects all measurements evaluated above. In Fig. 19(c) and 19(d) the raw and undersampled FROG data used as the experimental input for the reconstruction algorithm are plotted. It is obvious, that the undersampled data is substantially pixelled and we assume that this loss in resolution might yields some degree of freedom in the reconstructed pulses. However a quantitative discussion of this effect would go beyond the scope of this work.

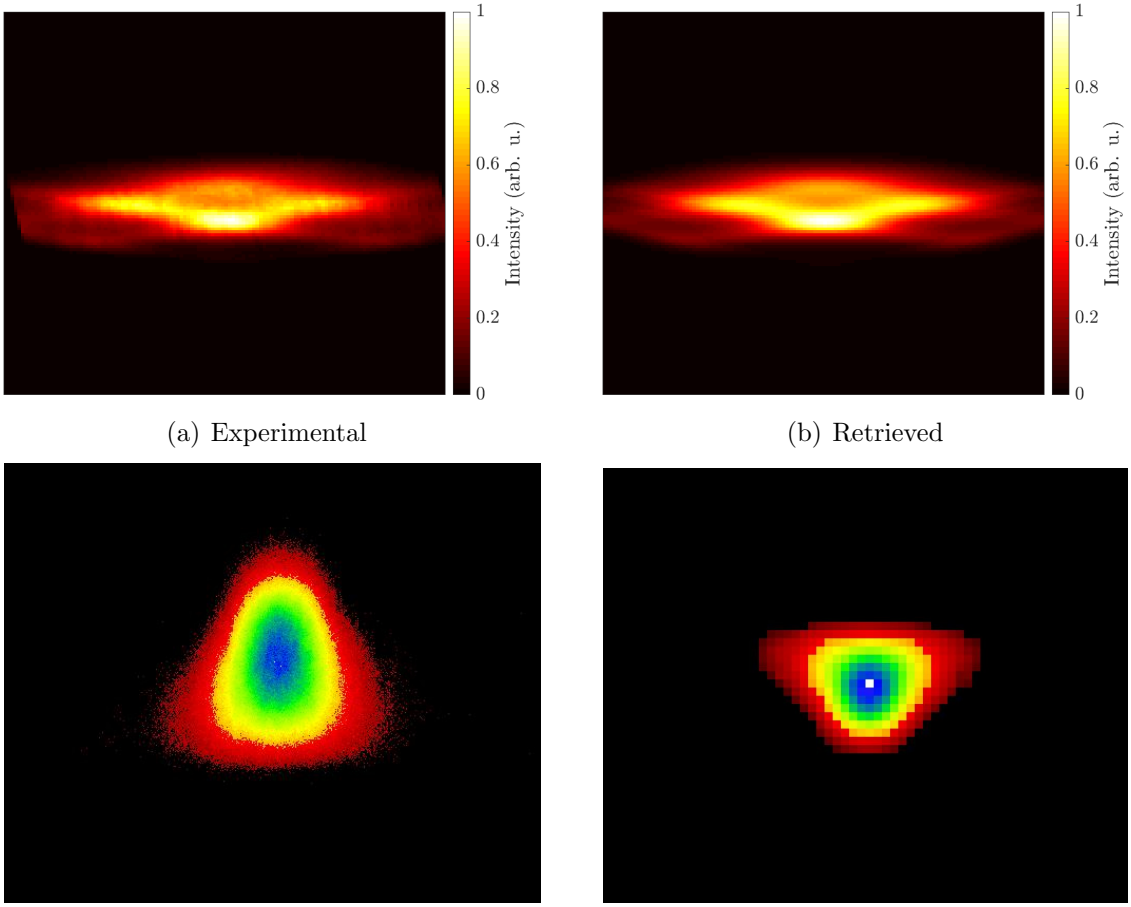

(a) Experimental

(b) Retrieved

(c) Raw

(d) Undersampled

Figure 19: Experimentally measured and retrieved FROG trace for the chirped mirrors (a) and (b). Raw data and undersampled FROG trace used in the reconstruction algorithm by the QuickFrog software. The rotation of the data is performed by the program itself.

5. Constructive Criticism

As we were the first experimentalists to conduct this advanced lab course experiment, many smaller and larger problems occured. We try to provide our criticism as detailed as possible in order to enable a better experiment and evaluation experience for our successors.

This experiment gave a useful insight into the challenges of everyday work with ultrashort laser pulses. It made the experimentalist well aware of possible issues that may arise. However, the abundant workload expected from the manual was challenging to fulfill and even with two semi-experienced experimentalists only a small fraction of the designated experiments could be performed during one day. Further detoriation came from the mirror and GRENOUILLE alignment which simply took most of the time during the experiment.

First of all, several experiments where hindered by a suboptimally aligned prism compressor which only allowed the compensation of a GDD up to $200\,\mathrm{fs}^2$. Thus, a reconstruction of the compressor is inevitable. By using an optical rail for the telecope lenses, one could substantially accelerate this part of the experiment.

Moreover, the thoughtful and thourough evaluation of the data involves not only advanced programming skills in programs like Matlab or Python, but moreover a large temporal effort in order to automize several evaluations, e.g., the fits for the spectral phase. The workload designated to 1.5 credits (6 Credits/4 experiments) is about 45 h and has been substantially exceeded by all of the experimentalists individually.

However, the largest complications occured with the QuickFrog software and its data files, where the restriction on naming (automatically performed by the program itself with only the time) being the smallest one. One had to guess which data could be found in the respective columns of the data files, moreover several values, e.g., the spatial chirp and pulse-front tilt are not exported to the data files but only in the form of screenshots. The general handling of the software during the experiment has been annoying due to the small displaying of the calculated value which can only be read while being directly in front of the screen.

In face of the negative criticism mentioned above one should not be tempted to depreciate the experiment. During conducting the experiment and data evaluation, a lot of useful knowledge could be acquired. It has been both enriching and entertaining and I would definitely recommend every physicists with some connection to ultrafast phenomena to conduct this experiment.

A. Adaption of experimental data

In the following, we try to explain which data has been adapted how and for which reason. First of all, the choosing of the sign of the phase, and thus the GDD, will be explained. Secondly, we will explain why four insertion lengths has been suspected to be falsely recorded and how they have been changed.

A.1. Sign of the spectral phase

1. For an insertion length of 27.5 mm, 28.0 mm and 28.5 mm the GDD must be positive according to the prism compressor theory which says that a higher insertion length yields a larger GDD.

2. For an insertion length 0f 27.26 mm the sign has not been changed as it must be negative in order to yield meaningful results for the GDD when inserting a material.

3. Measurement 2-20 is corrected in order to keep the same sign of the phase for nearby prism compressor positions.

4. When placing additional glass inside the beam path the GDD is expected to increase. The sign of the spectral phase is flipped for measurement 2-5 (15 mm BK7), 2-12 (5 mm BK7, tilted), 2-21 (GDD of MgF_2 telescope) and 3-24 (Wedge uncompensated).

5. For those materials which should be able to be compensated by the prism compressor, the sign of the GDD after compensation is chosen in accordance to the prism compressor theory (GDD(S)). The sign for measurement 2-6 (10 mm BK7 compensated) and 2-19 (5 mm BK7, tilted left and compensated) is flipped.

A.2. Insertion length of the second prism

As a full turn of the micrometer screw only yields 0.5 mm instead of 1 mm, the insertion length can easily be falsely recorded. As this yields a deviation of approximately 100 fs^2 for the GDD, we suspect four measurements to be flawed. As those errors have only been noted during data evaluation, only few data points have been affected and the mode of the advanced lab course does not favor reconducting a whole experiment, those errors have been corrected with consent from the assistant.

1. Measurement 2-3 (5 mm BK7 compensated) has been changed from 26.38 mm to 25.88 mm

2. Measurement 2-13 (5 mm MgF_2 compensated) has been changed from 26.79 mm to 26.29 mm

3. Measurement 2-16 (5 mm BK7, tilted left and compensated) has been changed from 26.33 mm to 25.83 mm

4. Measurement 2-19 (5 mm BK7, tilted right and compensated) has been changed from 26.34 mm to 25.84 mm

References

[1] The Royal Swedish Academy of Sciences. Nobelprize for ahmed zewail (femtochemistry). Press Release of the Royal Swedish Academy of Sciences, `https://www.nobelprize.org/nobel_prizes/chemistry/laureates/1999/press.html`, 1999.

[2] Martin Christopher Edward Galbraith. *Time-resolved spectroscopy with attosecond pulses and pulse trains: ultrafast relaxation in benzene cations*. PhD thesis, Freie Universität Berlin, 2016.

[3] A. McPherson, G. Gibson, H. Jara, U. Johann, T. S. Luk, I. A. McIntyre, K. Boyer, and C. K. Rhodes. Studies of multiphoton production of vacuum-ultraviolet radiation in the rare gases. *J. Opt. Soc. Am. B*, 4(4):595–601, Apr 1987.

[4] Fraunhofer Gesellschaft. Ultra-short laser pulses for science and industry. Research news, `https://www.fraunhofer.de/en/press/research-news/2012/may/ultra-short-laser-pulses-for-science-and-industry.html` as consulted online on 6th of october 2017, 16:50, 2012.

[5] Newport Corp. The effect of dispersion on ultrashort pulses. `https://www.newport.com/n/the-effect-of-dispersion-on-ultrashort-pulses` as consulted online on 3rd of November, 17:59.

[6] Patrick O'Shea, Mark Kimmel, Xun Gu, and Rick Trebino. Highly simplified device for ultrashort-pulse measurement. *Opt. Lett.*, 26(12):932–934, Jun 2001.

[7] Wolfgang Demtröder. *Experimentalphysik 2: Elektrizität und Optik*. Springer Verlag Berlin und Heidelberg, 2013.

[8] Rick Trebino. Springer, New York, 2000.

[9] Wolfgang Zinth Ursula Zinth. *Optik: Lichtstrahlen - Wellen - Photonen*. Oldenbourg Verlag München, 2013.

[10] Cosmin Lupulescu. *Femtosecond Analysis and Feedback Control of Molecular Processes in Organometallic and Alkaline Systems*. PhD thesis, Freie Universität Berlin, 2004.

[11] W. Sellmeier. Zur erklärung der abnormen farbenfolge im spectrum einiger substanzen. *Annalen der Physik und Chemie*, (219):272–282, 1871.

[12] Cosmin Lupulescu. *Femtosecond Analysis and Feedback Control of Molecular Processes in Organometallic and Alkaline Systems*. PhD thesis, Freie Universitaet Berlin, 2004.

[13] Léon Brillouin. Dover Publications Inc., 2003.

[14] Ultrafast Optics Group: Prof. Rick Trebino. Spatio-temporal distortions. `http://frog.gatech.edu/spatio-temporal-distortions.html`, as consulted online at 20th of November 2017, 21:01.

[15] Selcuk Akturk, Xun Gu, Erik Zeek, and Rick Trebino. Pulse-front tilt caused by spatial and temporal chirp. *Opt. Express*, 12(19):4399–4410, Sep 2004.

[16] Swamp Optics. Spatio-temporal distortions in pulses. `http://www.swampoptics.com/assets/tutorials-spatio-temporal-2015.pdf`, as consulted online at 15th of November 2017, 19:13.

[17] J. Hebling. Derivation of the pulse front tilt caused by angular dispersion. *Optical and Quantum Electronics*, 28(12):1759–1763, Dec 1996.

[18] DrBob on Wikipedia. Achromatic lens. `hhttps://commons.wikimedia.org/wiki/File:Lens6b.png`, as consulted online at 15th of November 2017, 19:06.

[19] Eugene Hecht, editor. Oldenbourg Verkag München Wien, 4th edition edition, 2005.

[20] E. Treacy. Optical pulse compression with diffraction gratings. *IEEE Journal of Quantum Electronics*, 5(9):454–458, Sep 1969.

[21] R. L. Fork, O. E. Martinez, and J. P. Gordon. Negative dispersion using pairs of prisms. *Opt. Lett.*, 9(5):150–152, May 1984.

[22] Jean-Claude Diels and Wolfgang Rudolph. Academic Press, Burlington, second edition edition, 2006.

[23] SCHOTT North America, Inc. *Schott Optical Glass Data Sheets*, 2015.

[24] Cristtel Y. RamÃrez-Corral, Martha Rosete-Aguilar, and Jesus Garduno-Mejia. Third-order dispersion in a pair of prisms. *Journal of Modern Optics*, 56(15):1659–1669, 2009.

[25] D. J. Kane and R. Trebino. Characterization of arbitrary femtosecond pulses using frequency-resolved optical gating. *IEEE Journal of Quantum Electronics*, 29(2):571–579, Feb 1993.

[26] Selcuk Akturk, Mark Kimmel, Patrick O'Shea, and Rick Trebino. Measuring pulse-front tilt in ultrashort pulses using grenouille. *Opt. Express*, 11(5):491–501, Mar 2003.

[27] C. Iaconis and I. A. Walmsley. Spectral phase interferometry for direct electric-field reconstruction of ultrashort optical pulses. *Opt. Lett.*, 23(10):792–794, May 1998.

[28] Swamp Optics. Intensity correlation. http://www.swampoptics.com/assets/tutorials_autocorrelation-2015.pdf, as consulted online at 15th of November 2017, 18:48.

[29] Ultrafast Optics Group: Prof. Rick Trebino. Interferometric autocorrelation/ultrafast optics course. http://frog.gatech.edu/images/slide9.jpg?crc=254718615, as consulted online at 28th of November 2017, 00:34.

[30] Zeekec at English Wikpedia. A schematic of a typical experimental, multishot shg frog setup. https://en.wikipedia.org/wiki/Frequency-resolved_optical_gating#/media/File:SHG_FROG.png as consulted online on 5rd of November, 19:28.

[31] Selcuk Akturk, Mark Kimmel, Patrick O'Shea, and Rick Trebino. Measuring spatial chirp in ultrashort pulses using single-shot frequency-resolved optical gating. *Opt. Express*, 11(1):68–78, Jan 2003.

[32] J. Hunter W.E. White K.W. DeLong, Rick Trebino. Frequency-resolved optical gating with the use of second-harmonic generation. *Journal of the Optical Society*, 11(11):2206–2215, 1994.

[33] Patrick A. Berry at English Wikpedia. A schematic of the grenouille setup. https://en.wikipedia.org/wiki/File:GRENOUILLE_long.JPG as consulted online on 5rd of November, 23:04.

[34] Sabine Steil. Instruction manual advanced lab course on spatial and temporal distortions of ultrashort light pulses. Versuchsanleitung, I. Physikalisches Institut, Fakultät der Physik, Friedrich-Hund-Platz 1, D-37075 Göttingen, 2017.

[35] Marilyn J. Dodge. Refractive properties of magnesium fluoride. *Appl. Opt.*, 23(12):1980–1985, Jun 1984.

[36] Thorlabs Inc. N-bk7 windows offered by thorlabs inc. online. https://www.thorlabs.de/NewGroupPage9.cfm?ObjectGroup_ID=1117., as consulted online at 26th of November 2017, 22:14.

[37] Torben Lennart Purz. Compression of femtosecond laser pulses using self-phase moulation in dielectric media. Bachelor's thesis at University of Göttingen, 2017.

[38] Thorlabs Inc. Chirped mirrors offered by thorlabs inc. online. https://www.thorlabs.com/newgrouppage9.cfm?objectgroup_id=3746, as consulted online at 14th of November 2017, 16:46.